IOP Publishing Journal of Physics: Condensed Matter
J. Phys.: Condens. Matter **29** (2017) 215702 (9pp) https://doi.org/10.1088/1361-648X/aa6b2a

Zn–VI quasiparticle gaps and optical spectra from many-body calculations

A Riefer[1], N Weber[1], J Mund[2], D R Yakovlev[2,3], M Bayer[2,3], Arno Schindlmayr[1], C Meier[1] and W G Schmidt[1]

[1] Department Physik, Universität Paderborn, 33095 Paderborn, Germany
[2] Experimentelle Physik 2, TU Dortmund, 44221 Dortmund, Germany
[3] Ioffe Institute, Russian Academy of Sciences, St. Petersburg 194021, Russia

E-mail: riefer@mail.upb.de

Received 10 January 2017, revised 22 March 2017
Accepted for publication 4 April 2017
Published 24 April 2017

Abstract

The electronic band structures of hexagonal ZnO and cubic ZnS, ZnSe, and ZnTe compounds are determined within hybrid-density-functional theory and quasiparticle calculations. It is found that the band-edge energies calculated on the G_0W_0 (Zn chalcogenides) or GW (ZnO) level of theory agree well with experiment, while fully self-consistent QSGW calculations are required for the correct description of the Zn 3d bands. The quasiparticle band structures are used to calculate the linear response and second-harmonic-generation (SHG) spectra of the Zn–VI compounds. Excitonic effects in the optical absorption are accounted for within the Bethe–Salpeter approach. The calculated spectra are discussed in the context of previous experimental data and present SHG measurements for ZnO.

Keywords: Zn–VI, Bethe–Salpeter, second-harmonic-generation, quasiparticle calculations

S Supplementary material for this article is available online

(Some figures may appear in colour only in the online journal)

1. Introduction

Wide-band-gap semiconductors have attracted technological interest because of their potential use for devices operating at high power and high temperature and because of the need for optical materials active in the blue-green spectral region. Among these materials, ZnS, ZnSe, ZnTe, as well as ZnO belong to the II–VI compounds, which are characterized by the existence of metal d bands inside the main valence band in column IIB. The electron correlation in the d shell renders the theoretical modeling of these compounds challenging. In the case of ZnO, the hexagonal wurtzite structure is most stable at ambient conditions and thus most common. ZnS, ZnSe, and ZnTe typically have a cubic zincblende crystal structure but can be also prepared as hexagonal crystals with wurtzite structure. These materials have received a lot of attention as blue lasing materials and could be used in the fabrication of heterostructures and optical wave guides [1–4]. Consequently, these materials were extensively studied. Their linear optical response [5–7] has been measured, and frequency-dependent second-harmonic-generation (SHG) coefficients have been determined for ZnS, ZnSe, and ZnTe [8]. SHG measurements for ZnO are restricted to specific wave lengths [9–12]. On the theoretical side, calculations within the independent-particle approximation (IPA) [13] as well as time-dependent density-functional theory (TDDFT) calculations are available for the Zn chalcogenides dielectric function [14] as well as for ZnO [7]. TDDFT was also used to determine the SHG in ZnS, ZnSe, and ZnTe [14], while the ZnO SHG was calculated within the IPA [15]. Quasiparticle energies obtained within the G_0W_0 approach were used by Sponza *et al* [16] to calculate the ZnO optical response. For ZnO a rigorous treatment of electron–hole excitations based on the Bethe–Salpeter equation (BSE) has also been performed. In this context, Laskowski and Christensen [17] as well as Esser and coworkers [7] used a scissors operator to adjust the DFT band gap to either the measured value or an average G_0W_0 correction, respectively, while Schleife *et al* [18, 19] used a so-called DFT + U + Δ method, where in addition to the scissors shift Δ the Coulomb-interaction term U is adjusted such that the

energy position of the *d* bands matches the hybrid-DFT based G_0W_0 results.

Given the interest in the II–VI compounds and the range of their potential application, a comparative study of their electronic properties and dielectric function based on a consistent, state-of-the-art treatment of many-body effects is certainly in order. This is the aim of the present work. Here we perform ground-state calculations based on hybrid-DFT [20–22] that provide a meaningful starting point to obtain electronic quasiparticle corrections. The latter are determined here within the GW_0 and *GW*, as well as the fully self-consistent QS*GW* approach [23–25]. While QS*GW* quasiparticle energies were calculated before for ZnS and ZnSe [26, 27], corresponding data for ZnTe and ZnO are—as far as we know—reported here for the first time. The linear optical response including electron–hole interaction is then obtained within the BSE [28–32], and the SHG spectra are determined on the level of the independent-(quasi)particle approximation [33–35]. Our work goes beyond previous optical-response calculations by starting from self-consistently obtained quasiparticle energies. The calculated results are discussed in the context of the available experimental data and previous calculations. In the case of ZnO, where only few experimental SHG data are available, measurements of the relative SHG intensities were made in order to allow for a comparison of theory with experiment.

2. Computational

In detail, the electronic ground state is obtained from hybrid-DFT using the HSE functional [20–22] as implemented in the vienna *ab initio* simulation package (VASP) [36]. The electron-ion interaction is described using the projector-augmented-wave (PAW) scheme [37–39]. The present calculations are based on the experimental lattice constants summarized in table 1.

The self-consistently calculated hybrid-DFT electronic structure is used as a starting point for quasiparticle calculations within the *GW* scheme [40], where the self-energy operator is expressed as a convolution of the single-particle propagator *G* and the dynamically screened Coulomb interaction *W*. Specifically, we perform one-shot G_0W_0 calculations, where the Green function and Coulomb potential are immediately obtained from the DFT electronic structure [25], as well as partially self-consistent GW_0 and *GW* calculations, where the energy eigenvalues are self-consistently updated in either *G* only or in both *G* and *W* [23]. In these schemes it is assumed that the quasiparticle wave functions are very similar to the Kohn–Sham wave functions. This assumption is dropped in the QS*GW* calculations, where the quasiparticle equation is solved self-consistently [24, 41]. We adopted the notation of Van Schilfgaarde *et al* [42] in order to distinguish the QS*GW* calculations performed here from the self-consistent iterative solution of the Dyson equation sometimes referred to as sc*GW* [43, 44]. The optical matrix elements in the QS*GW* calculations are updated using the perturbation-expansion-after-discretization finite-difference method according to Nunes and Gonze [45]. In all quasiparticle calculations described above, the energetically lowest 40 (80) states for ZnS, ZnSe, and ZnTe (ZnO) are updated.

Quasiparticle *GW* calculations are sensitive to the pseudopotentials and require careful convergence tests with respect to the number of electronic states as well as the Brillouin-zone (BZ) sampling, see, e.g. Klimeš *et al* [39]. An even denser **k**-point sampling is typically required for accurate calculations of the optical properties. On the other hand, quasiparticle calculations become expensive in memory and computation time with increasing **k**-point sampling. Therefore, different sets of numerical parameters are used here. The Zn 3*d* quasiparticle energies for cubic Zn compounds and ZnO are obtained using a $6 \times 6 \times 6$ and $6 \times 6 \times 3$ BZ sampling, respectively. Here we use energy cutoffs of 1000 eV and 600 eV for the HSE03 calculations and the determination of the response function in the *GW* calculations, respectively. The calculations of the self-energy include 1280 and 2650 states for cubic and hexagonal compounds, respectively. We perform calculations using both the standard and the *GW* PAW data sets provided with VASP. The latter are optimized with respect to the scattering properties at high energies but converge more slowly with respect to the number of bands [39]. The optical-response calculations require a denser BZ sampling (see below) and are therefore performed using standard PAW data sets and energy cutoffs of 400 eV and 200 eV for the HSE03 calculation and the determination of the response function in the *GW* calculation, respectively. The latter calculations include 160 and 320 states for cubic and hexagonal compounds, respectively. From the calculations using these different parameter sets, we estimate a numerical error bar of 0.1 and 0.2 eV for transitions energies close to the band gap and the 3*d* binding energies, respectively.

The calculation of the non-local response functions, see, e.g. [46], is simplified in the present work, since (i) we only consider translationally invariant systems and (ii) are interested in the response to electromagnetic waves with relatively small photon energies. The corresponding photon wave vectors are small compared to the extent of the Brillouin zone. Therefore, we restrict ourselves to the optical limit, i.e. vanishing wave vectors. Specifically, the long-wavelength limit in the longitudinal approximation [47] is used to determine the transition-matrix elements. The optical spectra are found to be well converged using regular, Γ-centered grids of $18 \times 18 \times 18$ and $18 \times 18 \times 9$ sampling points for the cubic and hexagonal Zn–VI compounds, respectively. These grids are used for optical-response and the corresponding quasiparticle calculations. The short-range Fock potential may be represented on a considerably coarser mesh in the BZ than other contributions to the Hamiltonian [48]. Here a reduction by a factor of three is found to reduce the computational effort considerably with no noticeable loss of accuracy. A transformation of the electron Bloch states to maximally-localized Wannier functions (MLWF) [49] is used to obtain the band dispersion from a finite number of sampling points along the BZ high-symmetry lines.

The linear optical response including electron–hole attraction and local-field effects is obtained from the Bethe–Salpeter equation using the numerical implementation described in

Table 1. Lattice constants a and c (in Å) used here as well as calculated band gaps E_g, Zn 3d binding energies (in eV, with standard (GW) PAW data sets), and high-frequency dielectric constants ϵ_∞ (ordinary and (extra-ordinary) values are given for ZnO). Band gaps and dielectric constants are calculated using $18 \times 18 \times 18$ ($18 \times 18 \times 9$) **k** points for cubic Zn compounds (ZnO). The respective sampling is reduced to $6 \times 6 \times 6$ ($6 \times 6 \times 3$) for the Zn 3d energies. See text for further parameters.

	ZnS	ZnSe	ZnTe	ZnO
a (c)	5.4102	5.6687	6.1035	3.2580 (5.2200)
E_g(Exp.)	3.66 .. 3.84[a]	2.7 .. 2.83[b]	2.18 .. 2.39[c]	3.26 .. 3.44[d]
E_g(HSE)	3.10	2.22	1.97	2.23
$E_g(G_0W_0)$	3.83	2.95	2.32	3.06
$E_g(GW_0)$	3.94	3.05	2.38	3.22
$E_g(GW)$	4.11	3.17	2.45	3.54
E_g(QSGW)	4.20	3.36	2.37	4.13
Zn 3d (Exp.)	9.03[e]	9.20[e], 8.9[f]	9.84[e], 9.1[f]	8.81[e], 8.5[f], 7.5[g]
Zn 3d (HSE)	7.44 (7.50)	7.85 (7.91)	8.43 (8.49)	5.89 (5.97)
Zn 3d (G_0W_0)	6.66 (7.24)	7.18 (7.62)	7.72 (8.15)	5.98 (6.21)
Zn 3d (GW_0)	6.57 (7.29)	7.09 (7.64)	7.57 (8.15)	6.05 (6.32)
Zn 3d (GW)	6.67 (7.41)	7.18 (7.74)	7.60 (8.22)	6.19 (6.45)
Zn 3d (QSGW)	7.49 (8.07)	7.82 (8.41)	8.23 (8.85)	6.39 (6.89)
ϵ_∞(Exp)	5.13[h]	5.4 .. 6.3[i]	7.1 .. 7.4[j]	3.60 .. 3.70 (3.66 .. 3.78)[k]
ϵ_∞(HSE)	5.15	5.97	7.37	3.54 (3.58)
$\epsilon_\infty(GW)$	4.57	5.30	6.64	3.13 (3.16)
ϵ_∞(QSGW)	4.42	5.03	6.57	3.00 (3.04)

[a] References [5, 54–56]
[b] References [54–58]
[c] References [55, 56, 59, 60]
[d] References [56, 61, 62]
[e] Reference [63]
[f] Reference [64]
[g] Reference [65]
[h] Reference [5, 66, 67]
[i] Reference [68] and references therein
[j] Reference [69, 70] and references therein
[k] Reference [71] and references therein

[28, 29, 31, 32]. The excitonic Hamiltonian is set up from the previously determined quasiparticle states and energies, and the screened electron–hole interaction is described by Bechstedt's model dielectric function [50]. The numerically converged representation of the ZnO critical-point contribution to the optical response is ensured by using a hybrid **k**-point mesh as suggested by Schleife *et al* [18]. Second-harmonic-generation spectra are calculated within the independent-particle or independent-quasiparticle approximation based on the hybrid-DFT or quasiparticle electronic structure, using the expressions derived by Leitsmann *et al* [33].

3. Results

Figure 1 shows the electronic band structures calculated here for the Zn chalcogenides and ZnO with the experimental lattice constants. Key parameters, such as the calculated band gaps in the various approximations as well as the calculated high-frequency dielectric constants ϵ_∞, are contained in table 1. As expected from the cubic symmetry, ZnS, ZnSe, and ZnTe show similar band dispersions. The band gaps vary, however. Here direct band gaps of 3.10, 2.22, and 1.97 eV are calculated within hybrid-DFT. These values are close to the hybrid-DFT results of Kresse *et al* [51] but clearly underestimate the respective experimental data also given in table 1. This underestimation of the Zn-chalcogenide band gaps is essentially lifted upon performing one-shot G_0W_0 calculations. This increases the band gaps by 20, 25, and 15% for ZnS, ZnS, and ZnTe, respectively, and yields band gaps that are within or very close to the scatter of measured values. It should be noted again that our non-self-consistent G_0W_0 calculations are based on HSE wave functions and energy eigenvalues and thus yield larger band gaps than previously reported calculations based on the local-density approximation or semilocal functionals [52].

A further moderate increase of the calculated band gaps is found by performing partially or fully self-consistent quasiparticle calculations. In the case of ZnS and ZnSe, we find that fully self-consistent QSGW calculations overestimate the measured band gaps severely by at least 0.4 and 0.5 eV, respectively. Similar effects have been reported for other materials [51, 53] and traced (i) to the neglect of excitonic effects in the screened Coulomb potential accompanied by the underestimation of the high-frequency dielectric constant ϵ_∞ (see comparison of calculated and measured values in table 1) as well as (ii) the neglect of zero-point motion and electron-phonon coupling, which redshift the electronic transition energies. The present results for ZnO show a similar trend as calculated for the Zn chalcogenides: the hybrid-DFT results clearly underestimate the measured band-gap values. This underestimation of more than 30% is essentially cured by one-shot G_0W_0 calculations. The agreement between experiment and

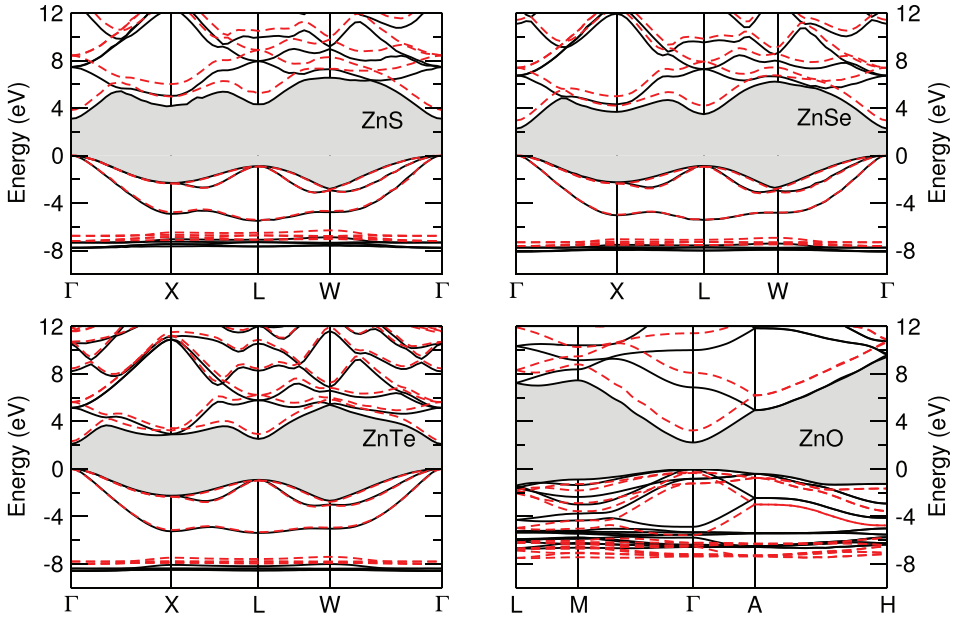

Figure 1. Band structures calculated within hybrid-DFT (HSE, solid black lines) and within the G_0W_0 and GW approach (red dashed lines) for the Zn chalcogenides and ZnO, respectively.

theory is further improved by partially including self-consistency effects: the results obtained from GW_0 and GW bracket the experimental findings for ZnO.

A more detailed comparison of the electronic structure calculated on different levels of theory with experimental data is made in the Supporting Information. It is found that the deviations between experiment and hybrid-DFT results for states close to the valence-band maximum are typically smaller than 0.5 eV and are in many cases reduced to less than 0.2 eV upon the inclusion of quasiparticle effects. The influence of self-consistency is minor: the results of one-shot G_0W_0 calculations differ from the fully self-consistent QSGW results mostly by less than 0.1 eV. This does not hold for the description of the Zn 3d states, however, as can be seen in table 1. In comparison with experiment, the HSE d-band positions are much too shallow for all compounds considered here. In the case of ZnO, the inclusion of quasiparticle effects improves the agreement between theory and experiment, but experiment and theory still deviate by more than one eV. For the Zn chalcogenides, the discrepancies between the measured d-band energies and the hybrid-DFT results are of the order of one eV but increase upon the inclusion of quasiparticle effects, at least if non-self-consistent or only partially self-consistent GW schemes are used. Fully self-consistent QSGW calculations yield d-band energies that are closer to the experimental data but still too shallow. The problem that the calculated 3d quasiparticle binding energies in the Zn–VI compounds are severely too low in comparison with experiment has been noted before, see, e.g. [23, 26, 27, 39, 72–79]. The deviations between G_0W_0 calculations and experiment have been attributed to self-consistency effects [72] assumed to arise from a strong hybridization between semicore and valence states, which may result in large non diagonal matrix elements of the self-energy operator [73]. GW calculations for ZnS and ZnSe were found to yield 3d energies that are slightly closer to experiment than the G_0W_0 values [74], and QSGW calculations [26, 27] improved the calculated energies further. Still, there remained noticeable discrepancies between theory and experiment, possibly related to missing electron–hole and/or vertex corrections [76], convergence issues [78] or the pseudopotentials [23, 39]. We perform calculations using both the standard and the GW PAW data sets provided with VASP. Both data sets give similar 3d energies (within 0.1 eV) in the HSE calculations for all Zn–VI compounds (see parenthetical values in table 1). However, the GW PAW data sets lower the 3d energies by about 0.5 eV in the quasiparticle calculations. The GW_0 calculations with these potentials essentially reproduce the data of [23]. If in addition the quasiparticle wave functions are updated, i.e. if QSGW calculations are performed, the 3d band energies are lowered further. This reduces the minimum deviation from the measured binding energies to 0.3, 0.5, 0.6, and 1.0 eV for ZnTe, ZnSe, ZnO, and ZnS, respectively.

Summarizing the band-structure findings discussed above, we find that HSE + G_0W_0 and HSE + GW reliably describe the electronic structure in the vicinity of the band edges of the Zn chalcogenides and ZnO, respectively, whereas the meaningful description of the Zn 3d states requires, however, the inclusion of self-consistency in the quasiparticle wave functions in addition to carefully devised PAW data. However, as described above, QSGW calculations clearly overestimate the measured band gaps. Therefore we use the HSE + G_0W_0 and HSE + GW electronic structures for the optical response calculations described below. The high-frequency dielectric constants calculated with hybrid-DFT are within the scatter of measured values. They are hence used to set up the model dielectric function [50], that describes the electron–hole interaction in the BSE Hamiltonian.

Figure 2 compares the Zn-chalcogenides optical absorption calculated within the BSE approach based on the HSE + G_0W_0 electronic structure with the experimental data from [5, 6].

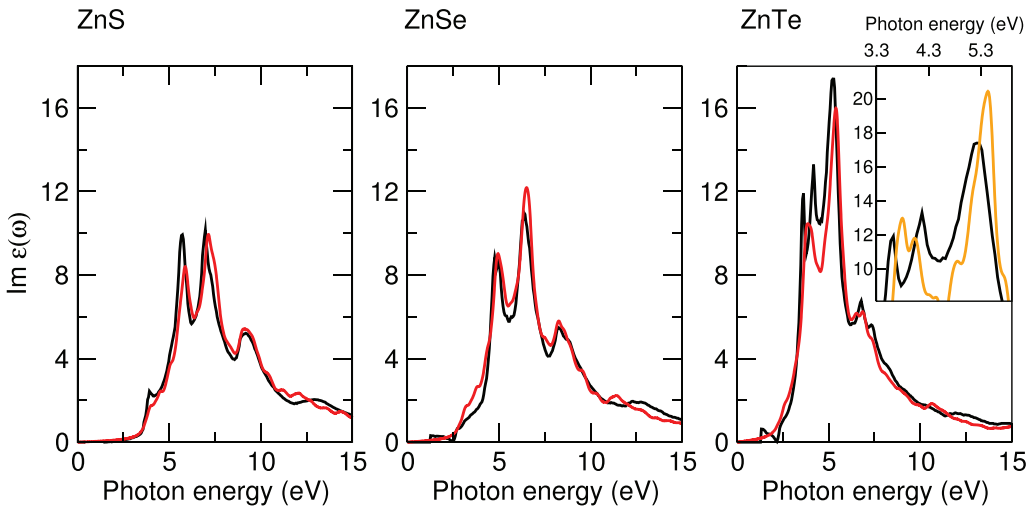

Figure 2. Dielectric functions for cubic ZnS, ZnSe, and ZnTe calculated on the HSE + G_0W_0 + BSE level of theory (red) in comparison to measured data from [5, 6] (black). The inset in (c) shows results where the broadening η is reduced from 0.2 to 0.1 eV (orange).

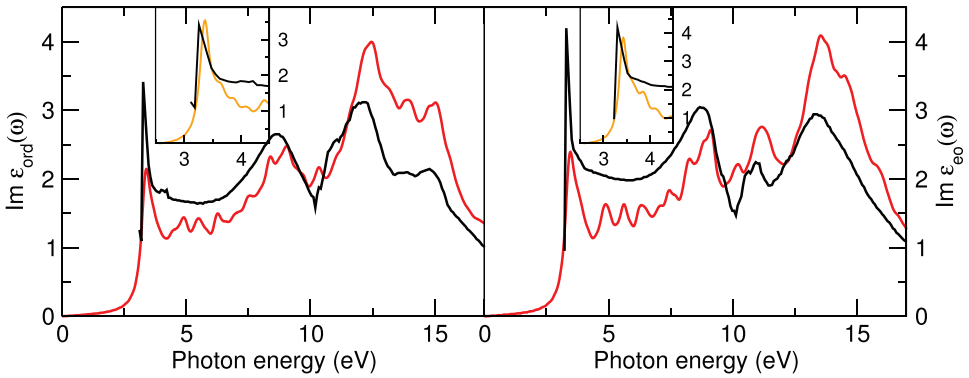

Figure 3. Ordinary and extraordinary ZnO dielectric functions calculated on the HSE + GW + BSE level of theory (red) in comparison to measured data (black) [7]. The insets show results where the broadening η is reduced from 0.2 to 0.1 eV (orange).

Generally, the agreement between the calculated and measured data is excellent. This holds in particular for the ZnS and ZnSe peak positions and line shapes. In the case of ZnTe, the calculations do not resolve the measured double-peak structure around 4 eV. This is not related to the broadening parameter in the calculations as can be seen from the inset in figure 2(c), where we reduce the broadening from 0.2 to 0.1 eV. We also verified that it is not related to spin-orbit coupling effects or the orbital character and energies of the quasiparticle states. Calculations where the BSE Hamiltonian is set up from QSGW energies and wave functions do not improve the agreement between theory and experiment. We mention that very recent TDDFT and BSE calculations for ZnTe by Grüning and Attaccalite [14] also indicate the occurrence of one rather than two peaks at 4 eV, similar to the present findings.

The modeling of the ZnO optical response is particularly challenging and requires a very well converged **k**-point set [18]. The present calculations start from quasiparticle energies calculated on a regular $18 \times 18 \times 9$ mesh, which is refined in the vicinity of the Brillouin-zone center by additional $9 \times 9 \times 5$ sampling points. Smoothly dispersing eigenenergies are obtained by a MLWF transformation. The weight with which the **k** points enter the calculations is normalized to their respective fraction of the BZ volume. Altogether, the rank of the exciton Hamiltonian solved here in the BSE amounts to 300 000. The ZnO optical absorption calculated for ordinary and extraordinary polarization is shown in figures 3(a) and (b). The calculations describe the measured data [7] very well, given the well-known difficulties to numerically model the ZnO optical response [16–18]. In particular, the sharp excitonic peak at the onset of the optical absorption is excellently reproduced. The oscillatory behavior of the absorption for photon energies between 4 and 8 eV might indicate the need for a further increase of the **k**-point sampling. This is at present computationally not feasible, however. On the other hand, temperature effects, not considered in the calculations, might have washed out part of the spectroscopic fine structure in the experiment. The calculations predict a higher absorption than experimentally measured for energies above 12 eV.

Obviously, HSE + G_0W_0 + BSE and HSE + GW + BSE calculations allow for a nearly perfect description of the II-VI-compound optical response. Slight deviations between experiment and theory might be related to temperature effects [53, 55, 80].

Second-harmonic-generation (SHG) spectra are calculated next. For computational reasons we are restricted to the

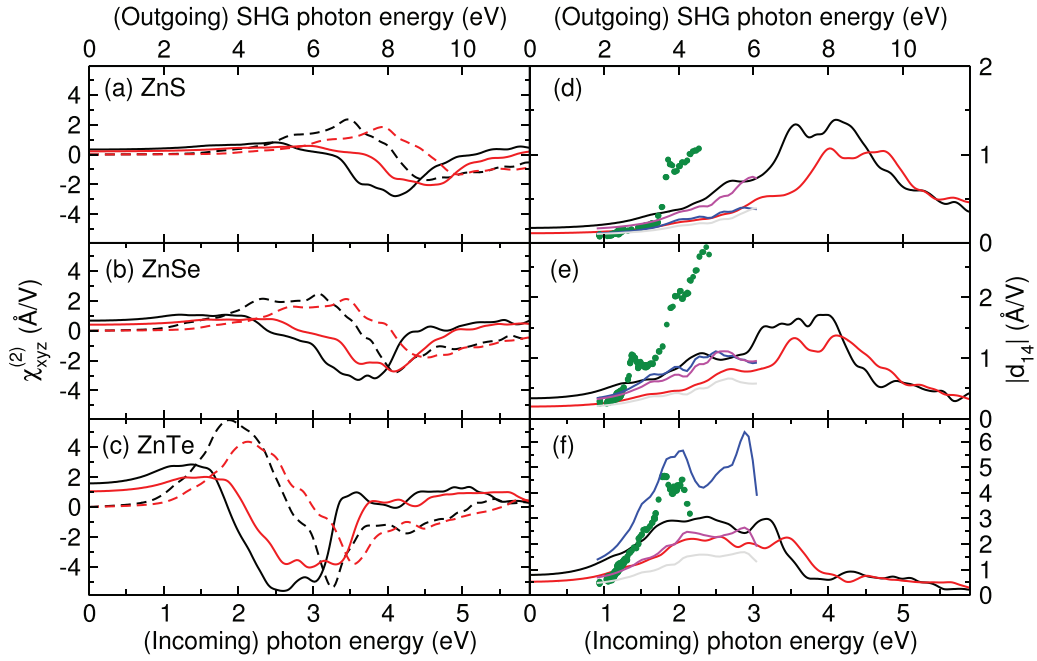

Figure 4. SHG spectra calculated for ZnS, ZnSe, and ZnTe within the IPA (IQA) are shown in black (red). Solid and dashed lines represent the real and imaginary parts of $\chi^{(2)}_{xyz}$. The energy axis refers to the frequency of the incident field. The comparison of the absolute values of the tensor element $|d_{14}| = |\chi^{(2)}_{xyz}|/2$ within the IPA and IQA with measurements from [8] (green symbols) is shown for ZnS (d), ZnSe (e), and ZnTe (f). A broadening of 0.15 eV is used. For comparison we also show very recent TDDFT calculations by Grüning *et al* [14], where the exchange-correlation part of the kernel is described using the GGA (grey), the bound-exciton model by Berger [81] (magenta), and the jellium-with-gap model [82] (blue). Note the different scales in (d)–(e).

independent-(quasi)particle approximation (IPA/IQA), i.e. the calculations are based on the HSE/HSE + G_0W_0 electronic structure. The real and imaginary parts of $\chi^{(2)}_{xyz}$ for the cubic Zn chalcogenides are shown in figure 4. As expected, contributions to $\mathrm{Im}\chi^{(2)}$ arise for fundamental photon energies above midgap. The IQA spectra are blue-shifted relative to the IPA results and are characterized by smaller intensities.

The calculated spectra are compared with measured $|\chi^{(2)}_{xyz}|$ data for ZnS, ZnSe, and ZnTe in figures 4(d)–(f). Overall, the calculations roughly reproduce the order of magnitude of the optical nonlinearities as well as the chemical trend observed experimentally of increasing SHG coefficients from ZnS over ZnSe to ZnTe. The detailed comparison with the data measured by Wagner *et al* [8] shows clear deviations with respect to line shapes and intensities, however. The onset of the spectra is overestimated, while the SHG strength is generally underestimated, in particular for ZnS and ZnSe. Overall, the IPA spectra agree better with experiment than the IQA spectra. This may indicate a strong influence of excitonic effects [83] on the optical nonlinearities neglected in the present calculations, which are, however, partially compensated by quasiparticle effects. This indicates that SHG calculations on the IPA level of theory are a meaningful starting point for the interpretation of the experiment.

Very recently, Grüning *et al* [14] presented TDDFT calculations for the nonlinear optical properties of bulk Zn chalcogenides. The calculated nonlinearities are smaller than the present IPA/IQA calculations and also smaller than experiment if the exchange-correlation kernel is described within the generalized gradient approximation (GGA), see the grey lines in figures 4(d)–(f). The calculated SHG coefficients increase, however, as soon as models are employed that approximate long-range correlation effects [81, 82], see the blue and magenta lines.

ZnO in the wurtzite structure has the point group 6mm and features three distinct SHG components $\chi^{(2)}_{xxz} = \chi^{(2)}_{xzx} = \chi^{(2)}_{yyz} = \chi^{(2)}_{yzy}$, $\chi^{(2)}_{zxx} = \chi^{(2)}_{zyy}$, and $\chi^{(2)}_{zzz}$. The corresponding calculations on the IPA/IQA level of theory are shown in figure 5. It can be seen that the sign of $\chi^{(2)}_{xzx}$ and $\chi^{(2)}_{zyy}$ differs from that of $\chi^{(2)}_{zzz}$ for photon energies above 1 eV, in agreement with the observation in [84]. The calculated intensities also agree with the scatter of experimental data: SHG measurements for a fundamental photon energy of 1.17 eV yield $|\chi^{(2)}_{zzz}|$ values of 0.04..0.13 Å/V [9], 0.14 Å/V [10], and 0.08..0.18 Å/V [11]. Considerably smaller values of 0.01..0.04 Å/V were measured for $|\chi^{(2)}_{zxx}|$ [9]. The ratio $|\chi^{(2)}_{zzz}|/|\chi^{(2)}_{zxx}|$ was determined to be 11 [10] and 4 [11]. The large scatter in the experimental data is related to the sample preparation, and in particular to the thickness of the ZnO films studied. In [9, 11] it was concluded that a significant part of the second-harmonic signal is generated at grain boundaries and interfaces. Therefore, the second-order susceptibilities observed in the very thin ZnO films are enhanced and can be larger than that of single-crystal ZnO.

In order to have a broader data base for the comparison between the present calculations and measured SHG intensities, we perform experiments using the setup schematically shown in figure 6. Specifically, the linearly polarized fundamental light with photon energy $\hbar\omega$ was generated by an

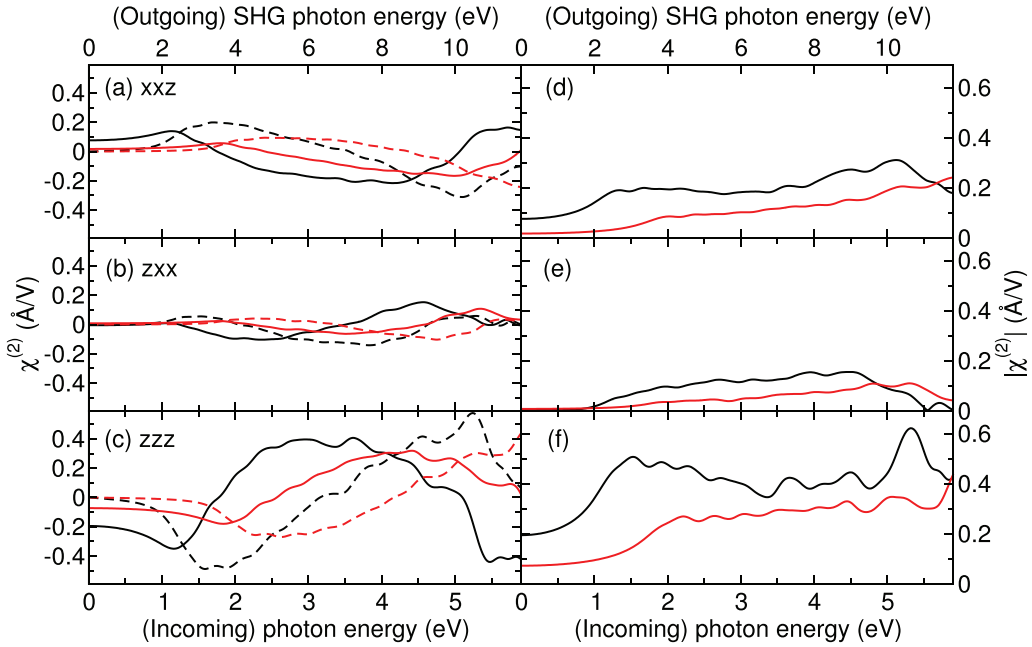

Figure 5. SHG spectra calculated for ZnO within the IPA (IQA) are shown in black (red). Solid and dashed lines represent the real and imaginary parts of $\chi^{(2)}$, respectively. A broadening of 0.2 eV is used.

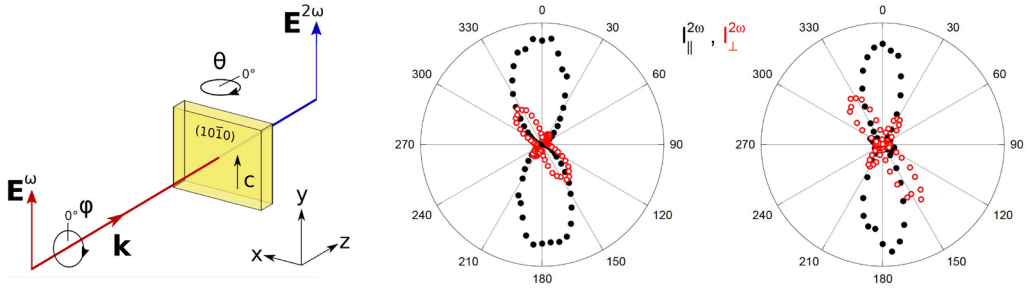

Figure 6. Sketch demonstrating the measurement geometry with a m-plane sample and indicated c axis (left). Here θ is the sample tilting angle and φ is the turning angle of $\mathbf{E}^{\omega(2\omega)}$ around $\mathbf{k}$. The angular dependence of the crystallographic SHG intensity ($\mathrm{I} = |\mathrm{P}|^2$) measured at $\theta = 0°$ for $\mathrm{T} = 300\,\mathrm{K}$ (middle) and $\mathrm{T} = 7\,\mathrm{K}$ (right) is exemplarily shown for a fundamental photon energy of 1.38 eV. Filled black and open red circles represent the geometries $\mathbf{E}^{2\omega} \| \mathbf{E}^{\omega}$ and $\mathbf{E}^{2\omega} \perp \mathbf{E}^{\omega}$, respectively.

optical parametric amplifier (OPA) tunable in the wavelength range of $315 - 2650\,\mathrm{nm}$ and emitting pulses of 3.3 ps duration. The OPA is pumped by 1030 nm of a Yb:KGW fs laser in combination with a second-harmonic bandwidth compressor. Depending on the wavelength output, powers of up to 1 W can be realised. Measurements are performed with several hundred μW. The SHG signal is collected in transmission geometry using two silica lenses with a focal length of 100 mm. The polarization angle ϕ is rotated for each excitation energy, and the resulting total polar intensity of the SHG, exemplarily shown in figure 6, is fitted to the expression

$$|\mathbf{P}^{2\omega} - (\mathbf{P}^{2\omega}\cdot\mathbf{k})\mathbf{k}|^2 = 4|\chi^{(2)}_{xxz}|^2\cos(\varphi)^2\sin(\varphi)^2 + |\chi^{(2)}_{zxx}|^2\cos(\varphi)^4 + |\chi^{(2)}_{zzz}|^2\sin(\varphi)^4 + 2\cos(\varphi)^2\sin(\varphi)^2\,\tau, \quad (1)$$

where $\tau = \mathrm{Re}[(\chi^{(2)}_{zzz})^*\chi^{(2)}_{zxx}]$ is determined from the calculations described above. This allows for determining the ratios $|\chi^{(2)}_{zzz}|/|\chi^{(2)}_{zxx}|$ and $|\chi^{(2)}_{zzz}|/|\chi^{(2)}_{xxz}|$ from the experimental data.

The comparison of the ratios measured here and in previous works with the present calculations is given in figure 7. The ratio $|\chi^{(2)}_{zzz}|/|\chi^{(2)}_{zxx}|$ calculated within the IQA varies between 6.5 and 8.7 for fundamental photon energies between 0 and 2 eV. The IPA ratio is noticeably larger. This is due to the small value of $\chi^{(2)}_{zxx}$, in the denominator of the ratio, for photon energies lower than 1 eV. Consequently, small changes in the two- and three-band contributions to $\mathrm{Re}[\chi^{(2)}_{zxx}]$ [33], differently affected by quasi particle corrections, are enhanced. The calculated $|\chi^{(2)}_{zzz}|/|\chi^{(2)}_{xxz}|$ ratio is smaller than $|\chi^{(2)}_{zzz}|/|\chi^{(2)}_{zxx}|$, irrespective of the methodology. For the photon energies considered here it amounts to 2..4. Comparing our calculations with present and previous measurements, we find good overall agreement: (i) The $|\chi^{(2)}_{zzz}|/|\chi^{(2)}_{zxx}|$ ratio is larger than the $|\chi^{(2)}_{zzz}|/|\chi^{(2)}_{xxz}|$ ratio both in theory and experiment, (ii) the measurements for $|\chi^{(2)}_{zzz}|/|\chi^{(2)}_{xxz}|$ are close to the present calculations, and (iii) while there is a strong scatter in the experimental data for $|\chi^{(2)}_{zzz}|/|\chi^{(2)}_{zxx}|$, we find nearly perfect agreement between the IPA calculations and the value determined for single crystals in [10]. We also mention that measured second-order susceptibility ratios are only little affected by temperature: the maximum deviation

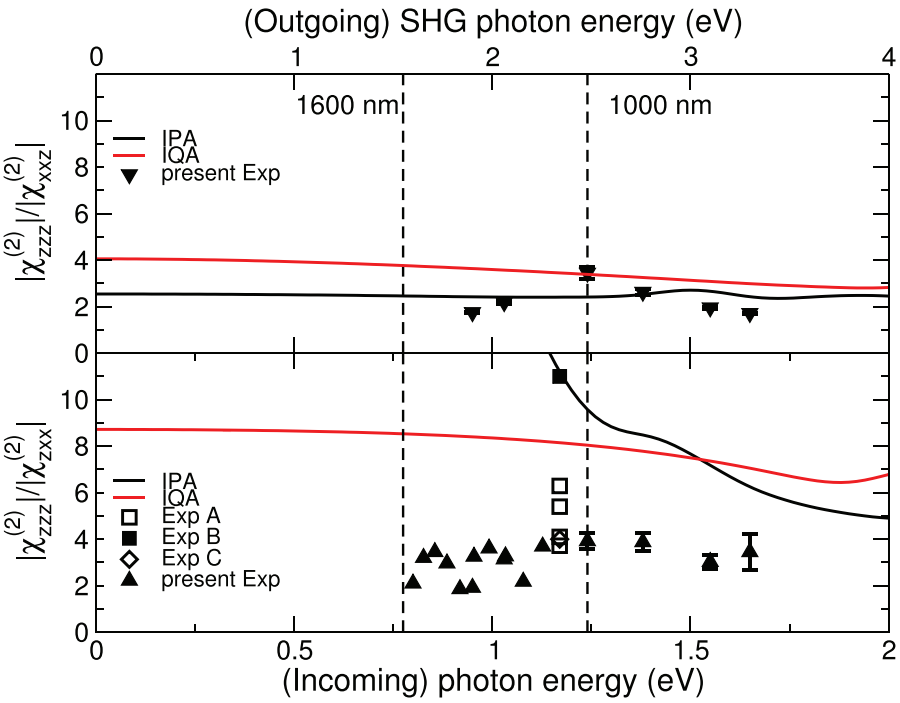

Figure 7. Measured and calculated ratio between SHG tensor components for ZnO. Solid (dashed) lines denote the present calculations within IQA (IPA). Triangles indicate the present experimental values determined from a fit to equation (1), while the squares and diamonds refer to experimental data A, B, and C from [9–11].

between the data measured at 7 K and at 300 K amounts to 16% and is therefore smaller than most differences between experiment and theory observed here. Given the scatter in the experimental data, the comparison between experiment and theory has to be made with caution. Nevertheless, comparing the IPA and IQA calculations with experiment, it appears that the IPA describes the measured ZnO data sligthly better. This agrees with the observations made above for the cubic Zn chalcogenides and might indicate that the excitonic influence on the optical nonlinearities partially compensates the quasiparticle effects.

4. Summary

In summary, self-consistent quasiparticle calculations based on hybrid-DFT are performed for cubic ZnS, ZnSe, and ZnTe as well as hexagonal ZnO. It is found that the band edges of the Zn chalcogenides are reliably described by one-shot G_0W_0 calculations on top of the hybrid-DFT electronic structure, while in the case of ZnO the inclusion of self-consistency effects in the Green function leads to an accurate description of the band gap. Fully self-consistent QSGW calculations are required for the correct modeling of the Zn 3d states, however. On the other hand, QSGW calculations overestimate the fundamental band gaps by typically half an eV, which is most likely related to excitonic effects in the screened Coulomb potential and the zero-point renormalization. Solving the Bethe–Salpeter equation starting from the HSE + G_0W_0 and the HSE + GW electronic structure results in optical absorption spectra for the Zn chalcogenides and ZnO, respectively, that excellently match the measured data. We also find the nonlinear optical spectra calculated within the independent-particle approximation to be in qualitative agreement with the measured data. The agreement does not improve upon the inclusion of quasiparticle effects, which may indicate a partial compensation of excitonic and self-energy effects.

Acknowledgments

We thank Claudio Attaccalite for helpful communications. The Deutsche Forschungsgemeinschaft (DFG) is acknowledged for financial support via the SFB/TRR 142, projects B01 and B04. The calculations were performed at the Paderborn Center for Parallel Computing (PC^2) and at the High Performance Computing Center in Stuttgart (HLRS).

References

[1] Haase M A, Qiu J, DePuydt J M and Cheng H 1991 *Appl. Phys. Lett.* **59** 1272–4
[2] Kinto H, Yagi M, Tanigashira K, Yamada T, Uchiki H and Iida S 1992 *J. Cryst. Growth* **117** 348–52
[3] Tamargo M, Brasil M, Nahory R, Martin R, Weaver A and Gilchrist H 1991 *Semicond. Sci. Technol.* **6** A8–13
[4] Chu S *et al* 2011 *Nat. Nanotechnol.* **6** 506–10
[5] Cardona M and Harbeke G 1965 *Phys. Rev.* **137** A1467–76
[6] Freeouf J L 1973 *Phys. Rev.* B **7** 3810–30
[7] Gori P, Rakel M, Cobet C, Richter W, Esser N, Hoffmann A, Del Sole R, Cricenti A and Pulci O 2010 *Phys. Rev.* B **81** 125207
[8] Wagner H P, Kühnelt M, Langbein W and Hvam J M 1998 *Phys. Rev.* B **58** 10494–501
[9] Cao H, Wu J Y, Ong H C, Dai J Y and Chang R P H 1998 *Appl. Phys. Lett.* **73** 572–4

[10] Wang G, Wong G K L and Ketterson J B 2001 *Appl. Opt.* **40** 5436–8
[11] Wang G, Kiehne G T, Wong G K L, Ketterson J B, Liu X and Chang R P H 2002 *Appl. Phys. Lett.* **80** 401–3
[12] Lafrentz M, Brunne D, Rodina A V, Pavlov V V, Pisarev R V, Yakovlev D R, Bakin A and Bayer M 2013 *Phys. Rev.* B **88** 235207
[13] Karazhanov S Z, Ravindran P, Kjekshus A, Fjellvåg H and Svensson B G 2007 *Phys. Rev.* B **75** 155104
[14] Grüning M and Attaccalite C 2016 *Phys. Chem. Chem. Phys.* **18** 21179–89
[15] Kong F and Jiang G 2009 *Physica* B **404** 2340–4
[16] Sponza L, Goniakowski J and Noguera C 2015 *Phys. Rev.* B **91** 075126
[17] Laskowski R and Christensen N E 2006 *Phys. Rev.* B **73** 045201
[18] Schleife A, Rödl C, Fuchs F, Furthmüller J and Bechstedt F 2009 *Phys. Rev.* B **80** 035112
[19] Schleife A and Bechstedt F 2012 *J. Mater. Res.* **27** 2180–9
[20] Heyd J, Scuseria G E and Ernzerhof M 2003 *J. Chem. Phys.* **118** 8207–15
[21] Heyd J and Scuseria G E 2004 *J. Chem. Phys.* **121** 1187–92
[22] Krukau A V, Vydrov O A, Izmaylov A F and Scuseria G E 2006 *J. Chem. Phys.* **125** 224106
[23] Shishkin M and Kresse G 2007 *Phys. Rev.* B **75** 235102
[24] Shishkin M, Marsman M and Kresse G 2007 *Phys. Rev. Lett.* **99** 246403
[25] Shishkin M and Kresse G 2006 *Phys. Rev.* B **74** 035101
[26] Kotani T, Van Schilfgaarde M and Faleev S V 2007 *Phys. Rev.* B **76** 165106
[27] Kotani T and Van Schilfgaarde M 2010 *Phys. Rev.* B **81** 125201
[28] Rödl C, Fuchs F, Furthmüller J and Bechstedt F 2008 *Phys. Rev.* B **77** 184408
[29] Fuchs F, Rödl C, Schleife A and Bechstedt F 2008 *Phys. Rev.* B **78** 085103
[30] Glutsch S, Chemla D S and Bechstedt F 1996 *Phys. Rev.* B **54** 11592
[31] Schmidt W G, Glutsch S, Hahn P H and Bechstedt F 2003 *Phys. Rev.* B **67** 085307
[32] Hahn P H, Schmidt W G and Bechstedt F 2001 *Phys. Rev. Lett.* **88** 016402
[33] Leitsmann R, Schmidt W G, Hahn P H and Bechstedt F 2005 *Phys. Rev.* B **71** 195209
[34] Riefer A, Sanna S, Gavrilenko A and Schmidt W 2012 *IEEE Trans. Ultrason. Ferroelectr. Freq. Control* **59** 1929–33
[35] Riefer A, Sanna S, Schindlmayr A and Schmidt W G 2013 *Phys. Rev.* B **87** 195208
[36] Kresse G and Furthmüller J 1996 *Comput. Mater. Sci.* **6** 15–50
[37] Blöchl P E 1994 *Phys. Rev.* B **50** 17953
[38] Kresse G and Joubert D 1999 *Phys. Rev.* B **59** 1758–75
[39] Klimeš J C V, Kaltak M and Kresse G 2014 *Phys. Rev.* B **90** 075125
[40] Hybertsen M S and Louie S G 1986 *Phys. Rev.* B **34** 5390–413
[41] Hahn P H, Schmidt W G and Bechstedt F 2005 *Phys. Rev.* B **72** 245425
[42] Van Schilfgaarde M, Kotani T and Faleev S 2006 *Phys. Rev. Lett.* **96** 226402
[43] Caruso F, Rinke P, Ren X, Scheffler M and Rubio A 2012 *Phys. Rev.* B **86** 081102
[44] Koval P, Foerster D and Sánchez-Portal D 2014 *Phys. Rev.* B **89** 155417
[45] Nunes R W and Gonze X 2001 *Phys. Rev.* B **63** 155107
[46] Calmels L, Inglesfield J, Crampin S, Arola E and Rasing T 2003 *Comput. Phys. Commun.* **151** 251–64
[47] Gajdoš M, Hummer K, Kresse G, Furthmüller J and Bechstedt F 2006 *Phys. Rev.* B **73** 045112
[48] Paier J, Marsman M, Hummer K, Kresse G, Gerber I C and Ángyán J G 2006 *J. Chem. Phys.* **124** 154709
[49] Mostofi A A, Yates J R, Pizzi G, Lee Y S, Souza I, Vanderbilt D and Marzari N 2014 *Comput. Phys. Commun.* **185** 2309–10
[50] Bechstedt F, Sole R D, Cappellini G and Reining L 1992 *Solid State Commun.* **84** 765–70
[51] Hinuma Y, Grüneis A, Kresse G and Oba F 2014 *Phys. Rev.* B **90** 155405
[52] Friedrich C, Betzinger M, Schlipf M, Blügel S and Schindlmayr A 2012 *J. Phys.: Condens. Matter* **24** 293201
[53] Riefer A, Friedrich M, Sanna S, Gerstmann U, Schindlmayr A and Schmidt W G 2016 *Phys. Rev.* B **93** 075205
[54] Theis D 1977 *Phys. Status Solidi* b **79** 125–30
[55] Pässler R *et al* 1999 *J. Appl. Phys.* **86** 4403–11
[56] Strehlow W H and Cook E L 1973 *J. Phys. Chem. Ref. Data* **2** 163–200
[57] Ves S and Str K 1985 *Solid State Commun.* **56** 479–83
[58] Aven M, Marple D T F and Segall B 1961 *J. Appl. Phys.* **32** 2261–5
[59] Nahory R E and Fan H Y 1967 *Phys. Rev.* **156** 825–33
[60] Riccius H and Turner R 1968 *J. Phys. Chem. Solids* **29** 15–8
[61] Park Y S, Litton C W, Collins T C and Reynolds D C 1966 *Phys. Rev.* **143** 512–9
[62] Ebina A, Koda T and Shionoya S 1965 *J. Phys. Chem. Solids* **26** 1497–506
[63] Ley L, Pollak R A, McFeely F R, Kowalczyk S P and Shirley D A 1974 *Phys. Rev.* B **9** 600–21
[64] Vesely C J, Hengehold R L and Langer D W 1972 *Phys. Rev.* B **5** 2296–301
[65] Powell R A, Spicer W E and McMenamin J C 1971 *Phys. Rev. Lett.* **27** 97–100
[66] Reynolds D C, Litton C W and Collins T C 1965 *Phys. Status Solidi* B **12** 3–55
[67] Czyzak S J, Baker W M, Crane R C and Howe J B 1957 *J. Opt. Soc. Am.* **47** 240–3
[68] Madelung O, Rössler U and Schulz M (ed) 1999 *Zinc Selenide (ZnSe) Dielectric Constants* (Berlin: Springer) pp 1–6
[69] Madelung O, Rössler U and Schulz M (ed) 1999 *Zinc Telluride (ZnTe) Dielectric Constants* (Berlin: Springer) pp 1–5
[70] Constable E and Lewis R A 2012 *J. Appl. Phys.* **112** 063104
[71] Ashkenov N *et al* 2003 *J. Appl. Phys.* **93** 126–33
[72] Rohlfing M, Krüger P and Pollmann J 1998 *Phys. Rev.* B **57** 6485–92
[73] Oshikiri M and Aryasetiawan F 1999 *Phys. Rev.* B **60** 10754–7
[74] Luo W, Ismail-Beigi S, Cohen M L and Louie S G 2002 *Phys. Rev.* B **66** 195215
[75] Usuda M, Hamada N, Kotani T and Van Schilfgaarde M 2002 *Phys. Rev.* B **66** 125101
[76] Rinke P, Qteish A, Neugebauer J, Freysoldt C and Scheffler M 2005 *New J. Phys.* **7** 126
[77] Miyake T, Zhang P, Cohen M L and Louie S G 2006 *Phys. Rev.* B **74** 245213
[78] Shih B C, Xue Y, Zhang P, Cohen M L and Louie S G 2010 *Phys. Rev. Lett.* **105** 146401
[79] Lim L Y, Lany S, Chang Y J, Rotenberg E, Zunger A and Toney M F 2012 *Phys. Rev.* B **86** 235113
[80] Olguín D, Cardona M and Cantarero A 2002 *Solid State Commun.* **122** 575–89
[81] Berger J A 2015 *Phys. Rev. Lett.* **115** 137402
[82] Trevisanutto P E, Terentjevs A, Constantin L A, Olevano V and Sala F D 2013 *Phys. Rev.* B **87** 205143
[83] Luppi E, Hübener H and Véniard V 2010 *J. Chem. Phys.* **132** 241104
[84] Shen Y R 2003 *The Principles of Nonlinear Optics* (Hoboken, NJ: Wiley-Interscience)

Supporting information for:

Zn-VI quasiparticle gaps and optical spectra from many-body calculations

A. Riefer[1], N. Weber[1], J. Mund[2], D. R. Yakovlev[2,3], M. Bayer[2,3], Arno Schindlmayr[1], C. Meier[1], W. G. Schmidt[1]

[1] Department Physik, Universität Paderborn, 33095 Paderborn, Germany
[2] Experimentelle Physik 2, TU Dortmund, 44221 Dortmund, Germany
[3] Ioffe Institute, Russian Academy of Sciences, St Petersburg 194021, Russia

E-mail: `riefer@mail.upb.de`

22 March 2017

In Table 1 below a comparison of the electronic structure calculated here on different levels of theory with experimental data is made. The calculated electron binding energies at high-symmetry **k** points are compared with photoelectron-spectroscopy measurements [1, 2].

References

[1] L. Ley, R. A. Pollak, F. R. McFeely, S. P. Kowalczyk, and D. A. Shirley. Total valence-band densities of states of III-V and II-VI compounds from x-ray photoemission spectroscopy. *Phys. Rev. B*, 9:600–621, Jan 1974.

[2] C. J. Vesely, R. L. Hengehold, and D. W. Langer. uv photoemission measurements of the upper d levels in the IIB-VIA compounds. *Phys. Rev. B*, 5:2296–2301, Mar 1972.

[3] J. Chelikowsky, D. J. Chadi, and Marvin L. Cohen. Calculated valence-band densities of states and photoemission spectra of diamond and zinc-blende semiconductors. *Phys. Rev. B*, 8:2786–2794, Sep 1973.

[4] U. Rössler. Energy bands of hexagonal ii-vi semiconductors. *Phys. Rev.*, 184:733–738, Aug 1969.

[5] R. A. Powell, W. E. Spicer, and J. C. McMenamin. Location of the Zn3d states in zno. *Phys. Rev. Lett.*, 27:97–100, Jul 1971.

Table 1. Electron binding energies in eV at high-symmetry **k** points with respect to the valence-band maximum, notation adapted from Refs. [3, 4].

	L_3	X_5	W_2	W_1	$X_3(L_1)$	X_3-X_1
ZnS						
Exp.	1.4[a]	2.5[a]	3.0[a]	4.9[a]	5.5[a]	6.5[a]
HSE03	0.90	2.31	2.94	4.77	4.91 (5.50)	8.00
G_0W_0	0.92	2.32	2.90	4.62	4.68 (5.34)	7.42
GW_0	0.92	2.34	2.93	4.68	4.72 (5.40)	7.33
GW	0.94	2.38	2.97	4.75	4.81 (5.51)	7.42
QSGW	0.93	2.35	3.02	4.75	4.92 (5.51)	7.30
ZnSe						
Exp.	1.3[a]	2.1[a]	2.6[a]	5.2[a]	5.6[a]	6.9[a]
HSE03	0.90	2.28	2.96	4.86	5.06 (5.45)	8.08
G_0W_0	0.93	2.31	2.91	4.72	4.9 (5.33)	7.48
GW_0	0.94	2.34	2.96	4.79	4.95 (5.39)	7.36
GW	0.95	2.37	2.86	4.83	5.04 (5.50)	7.38
QSGW	0.93	2.33	2.99	4.84	5.06 (5.45)	7.38
ZnTe						
Exp.	1.1[a]	2.4[a]	2.7[a]	5.1[a]	5.5[a]	6.1[a]
HSE03	0.94	2.28	2.97	5.09	5.29 (5.43)	6.16
G_0W_0	0.97	2.32	3.00	4.92	5.11 (5.28)	5.60
GW_0	0.97	2.34	3.02	4.98	5.15 (5.33)	5.44
GW	0.98	2.37	3.04	5.05	5.23 (5.41)	5.45
QSGW	0.98	2.35	3.08	5.04	5.24 (5.40)	5.53
ZnO	U_1-U_1	U_2 -U_2	U_3	U_4	Γ_1-Γ_6	Γ_3
Exp.						5.2[a]
HSE03	2.89	3.27	3.98	1.09	0.82	4.88
G_0W_0	2.93	3.28	4.10	1.17	0.89	4.93
GW_0	2.97	3.33	4.14	1.18	0.90	4.99
GW	3.02	3.40	4.23	1.20	0.92	5.11
QSGW	3.38	3.44	4.15	0.76	0.89	5.19

[a] Ref. [1]
[b] Ref. [2]
[c] Ref. [5]